Atmos. Chem. Phys. Discuss., 12, 23261–23290, 2012
www.atmos-chem-phys-discuss.net/12/23261/2012/
doi:10.5194/acpd-12-23261-2012

Atmospheric Chemistry and Physics Discussions

Global and regional temperature-change potentials for near-term climate forcers

W. J. Collins[1], M. M. Fry[2], H. Yu[3,4], J. S. Fuglestvedt[5], D. T. Shindell[6], and J. J. West[2]

[1]Met Office Hadley Centre, FitzRoy Road, Exeter, Devon, EX1 3PB, UK
[2]Department of Environmental Sciences and Engineering, The University of North Carolina at Chapel Hill, 146B Rosenau Hall, CB #7431, Chapel Hill, North Carolina, 27599, USA
[3]Earth System Science Interdisciplinary Center, University of Maryland, College Park, Maryland, 20740, USA
[4]Earth Science Directorate, NASA Goddard Space Flight Center, Greenbelt, Maryland, 20771, USA
[5]Center for International Climate and Environmental Research – Oslo (CICERO), P.O. Box 1129 Blindern, 0318 Oslo, Norway
[6]NASA Goddard Institute for Space Studies, 2880 Broadway, New York, New York, 10025, USA

Received: 30 July 2012 – Accepted: 24 August 2012 – Published: 7 September 2012

Correspondence to: W. J. Collins (bill.collins@metoffice.gov.uk)

Published by Copernicus Publications on behalf of the European Geosciences Union.

Abstract

We examine the climate effects of the emissions of near-term climate forcers (NTCFs) from 4 continental regions (East Asia, Europe, North America and South Asia) using radiative forcing from the task force on hemispheric transport of air pollution source-receptor global chemical transport model simulations. These simulations model the transport of 3 aerosol species (sulphate, particulate organic matter and black carbon) and 4 ozone precursors (methane, nitric oxides (NO_x), volatile organic compounds and carbon monoxide). From the equilibrium radiative forcing results we calculate global climate metrics, global warming potentials (GWPs) and global temperature change potentials (GTPs) and show how these depend on emission region, and can vary as functions of time. For the aerosol species, the GWP(100) values are -37 ± 12, -46 ± 20, and 350 ± 200 for SO_2, POM and BC respectively for the direct effects only. The corresponding GTP(100) values are -5.2 ± 2.4, -6.5 ± 3.5, and 50 ± 33.

This analysis is further extended by examining the temperature-change impacts in 4 latitude bands. This shows that the latitudinal pattern of the temperature response to emissions of the NTCFs does not directly follow the pattern of the diagnosed radiative forcing. For instance temperatures in the Arctic latitudes are particularly sensitive to NTCF emissions in the northern mid-latitudes. At the 100-yr time horizon the ARTPs show NO_x emissions can have a warming effect in the northern mid and high latitudes, but cooling in the tropics and Southern Hemisphere. The northern mid-latitude temperature response to northern mid-latitude emissions of most NTCFs is approximately twice as large as would be implied by the global average.

1 Introduction

Through their influence on air quality pollutants ozone and particulate matter, the emissions of reactive gases and aerosols can affect human and ecosystem health (HTAP, 2010). They can also affect climate through the burdens of ozone, methane

ACPD
12, 23261–23290, 2012

and aerosols, having both cooling and warming impacts. Because they have short lifetimes, the climate impacts are significant in the near term and we will use "near-term climate forcer (NTCF)" to refer to them. For nearly all these pollutants the global and local climate impacts depend on the location of their emission.

UNEP and WMO (2011) and Shindell et al. (2012) suggested that the mitigation of ozone precursors and black carbon would be attractive for both air quality and climate on a 30-yr timescale provided it is not at the expense of CO_2 mitigation. Typical air quality policies target both warming and cooling species and tend to have an overall detrimental effect on climate (in terms of surface temperature). Therefore it is important to understand how effects of NTCFs vary by location of emissions, when air quality policies are considered, as well as for climate policies that affect both short and long lived species (Berntsen et al., 2006).

The NTCFs we will consider in this paper are primary aerosols, secondary aerosol precursors, methane and ozone precursors. Some halogenated species have short lifetimes and are therefore NTCFs, but we will not consider them here. NTCFs with lifetimes longer than the interhemispheric mixing time (such as methane) are reasonably well mixed, with the concentrations and radiative forcing pattern independent of the emission location. Species with shorter lifetimes such as ozone and aerosols have heterogeneous distributions and radiative forcing patterns that are dependent on the emission location (Fuglestvedt et al., 1999; Berntsen et al., 2005; Naik et al., 2005; Fry et al., 2012; Yu et al., 2012). The surface temperature response doesn't follow the spatial details of the radiative forcing pattern, rather it smoothes out the pattern over scales of $\sim$ 3500 km in the meridional direction and over 12 000 km in the zonal direction (Shindell et al., 2010).

In this paper, we use radiative forcing (RF) estimates from the Task Force on Hemispheric Transport of Air Pollution (HTAP) Source-Receptor global chemical transport model (CTM) simulations (HTAP, 2010). From these we calculate the responses in global mean surface temperature as functions of time for emissions of different components in different regions and normalise by the corresponding response for CO_2 to

ACPD
12, 23261–23290, 2012

derive global temperature-change potentials (Shine et al., 2005). We also go beyond looking at global mean values for the response and use the recently introduced concept of the regional temperature-change potential (Shindell and Faluvegi, 2010; Shindell et al., 2012) to quantify the impacts of regional pollutant emissions on temperatures in broad latitude bands.

2 Methodology

The basic data needed as input to the GWP and GTP calculations can be derived from the equilibrium radiative forcing responses of chemistry transport models to step changes in emissions. As part of the HTAP study (HTAP, 2010) an ensemble of chemistry transport models carried out experiments reducing the emissions of (anthropogenic) ozone or aerosol precursors by 20% in four Northern Hemisphere continental regions (North America (NA, 15°–55° N, 60°–125° W), Europe (EU, 25°–65° N, 10° W–50° E), East Asia (EA, 15°–50° N, 95°–160° E), and South Asia (SA, 5°–35° N, 50°–95° E)). The effects of regional ozone precursor emission changes (NO_x, CO, NMVOCs, methane) on ozone and methane concentrations were calculated by Fiore et al. (2009). The consequent net radiative forcing impacts from an ensemble of 11 of the CTMs were calculated by Fry et al. (2012). The changes in radiative forcing due to the emissions of SO_2, primary particulate organic matter (PM) and black carbon (BC) were calculated by Yu et al. (2012) from an ensemble of 9 models.

Because of the time needed for methane to equilibrate to emissions changes, methane concentrations were fixed globally to 1760 ppb (nmol mol^{-1}) for all experiments except for the methane perturbation experiment in which it was reduced to 1408 ppb. The impacts of ozone precursor emissions on global methane and long-term ozone responses were calculated analytically from the methane loss by tropospheric OH diagnostic reported by each CTM (Fiore et al., 2009; Fry et al., 2012).

Fry et al. (2012) used the GFDL radiative transfer model (GFDL GAMDT, 2004) to calculate the gridded, stratospheric-adjusted net radiative fluxes (incoming shortwave

ACPD
12, 23261–23290, 2012

minus outgoing longwave) at steady state due to changes in methane, ozone, and sulphate aerosol. The 3-D concentration fields were from the multi-model mean along with the mean ±1 standard deviation. The RTM simulations exclude aerosol-cloud interactions and the internal mixing of aerosols.

Yu et al. (2012) applied normalised direct radiative forcings (NDRFs) calculated with the GOCART model (Yu et al., 2004) to the aerosol optical depths (AODs) from each model. The NDRFs were applied on a $2^{\circ} \times 2.5^{\circ}$ degree grid for each month of the year for each of the three components (SO_4, POM, BC). No aerosol-cloud interactions were included and the aerosols were assumed to be externally mixed in that the concentration of one did not affect the radiative forcing of another.

3 Global metrics

3.1 Global warming potentials

The absolute global warming potential (AGWP) is defined (e.g. Fuglestvedt et al., 2010) as the integrated radiative forcing over a time horizon H due to a 1 kg pulse emission of a species and has units $\mathrm{W\,m^{-2}\,yr\,kg^{-1}}$. For a species with an exponential decay with lifetime α, $\mathrm{AGWP}(H) = A\alpha(1 - \exp(-H/\alpha))$ where A is the specific radiative forcing (radiative forcing per kg atmospheric burden). AGWP is typically normalised by the equivalent AGWP for CO_2 to give a dimensionless quantity GWP.

For the aerosol species, the lifetimes are sufficiently short that the atmospheric burdens rapidly reach equilibrium after a step change in emission. The equilibrium radiative forcings F per emission change E for each species (F/E) (e.g. Table 6 of Yu et al., 2012) is equal to $A\alpha$. Hence, provided that the time horizon chosen is much longer than the lifetime of the aerosol ($H \gg \alpha$), the AGWP is also simply equal to the equilibrium response to a unit step change in emissions and is independent of the time horizon. A similar argument was made in Bond et al. (2011) where they introduced the specific forcing pulse SFP (units $\mathrm{J\,kg^{-1}}$). For short-lived species ($\alpha \ll H$) the global

ACPD
12, 23261–23290, 2012

SFP is simply the AGWP multiplied by the surface area of the Earth and the number of seconds in a year.

The AGWP is a measure of the globally-averaged net radiative effect of an emission pulse, but the emissions themselves do not need to be globally emitted. Emissions from different regions may have different lifetimes and the specific radiative forcings may be regionally dependent leading to a dependence of AGWP on the emitting region. AGWPs for SO_2, POM and BC are listed for the 4 HTAP regions in Table 1. These are the same values listed in Yu et al. (2012) Table 6 with a change of units. AGWPs for SO_2 and POM are negative reflecting the cooling impact. The values for EA are slightly smaller than for the other continents due to more rapid removal of the aerosols and lower oxidation efficiency. In contrast, BC emissions have positive AGWPs, and the values for EU are slightly larger than for the other continents as these absorbing aerosols are advected over the brighter surfaces of the Arctic. The GWP(100) values can be derived by normalising by the $\mathrm{AGWP}^{\mathrm{CO_2}}(100)$ and give -37 ± 12, -46 ± 20, and 350 ± 200 for SO_2, POM and BC, respectively. These are of slightly lower magnitude than in Fuglestvedt et al. (2010), but within the uncertainty ranges.

The decay time for a methane perturbation is around 12 yr, hence for policy-relevant time horizons of 20 or 30 yr the criterion ($\alpha \ll H$) no longer holds. For methane, the HTAP experiments were based on a global change in the methane concentration rather than regional emission changes to save running the chemistry models to equilibrium. Here the direct AGWP is again given by $\frac{F_{\mathrm{CH_4}}^{\mathrm{CH_4}}}{E^{\mathrm{CH_4}}}\left(1-\exp(-H/f\alpha^{\mathrm{CH_4}})\right)$ where $F_{\mathrm{CH_4}}^{\mathrm{CH_4}}$ is the methane forcing diagnosed from the methane change experiment using the Ramaswamy et al. (2001) formula. The factor f accounts for the effect of methane on its own lifetime (Prather et al., 1996). The implied emissions necessary to cause this change in concentration are given by $E^{\mathrm{CH_4}} = \Delta B_{\mathrm{CH_4}}/f\alpha^{\mathrm{CH_4}}$ where $\Delta B^{\mathrm{CH_4}}$ is the change in methane burden. In the HTAP methane perturbation experiment (SR2) where methane was decreased from 1760 ppb to 1408 ppb, $\Delta B_0^{\mathrm{CH_4}} = 979$ Tg,

ACPD
12, 23261–23290, 2012

$\alpha^{CH_4} = 8.7 \pm 1.3\,\text{yr}$, $f = 1.34 \pm 0.05$ (Fiore et al., 2009) giving an implied emission of $-84\,\text{Tg}\,\text{yr}^{-1}$. Methane is an ozone precursor, it affects the oxidation rate of SO_2 to sulphate aerosol and generates water vapour (this is only important in the stratosphere). Two indirect forcings due to changes in ozone $F^{O_3}_{CH_4}$ and sulphate $F^{SO_4}_{CH_4}$ were calculated in Fry et al. (2012), we also assume a stratospheric water vapour forcing $F^{H_2O}_{CH_4}$ equal to 15 % ± 10 % of the direct methane forcing (Forster et al., 2007). The total direct + indirect AGWP from methane (excluding CO_2) is therefore

$$\text{AGWP}^{CH_4} = \left(F^{CH_4}_{CH_4} + F^{O_3}_{CH_4} + F^{SO_4}_{CH_4} + F^{H_2O}_{CH_4}\right) \frac{f\alpha^{CH_4}}{\Delta B_{CH_4}} \left(1 - \exp(-H/f\alpha^{CH_4})\right). \quad (1)$$

Ozone precursors have a short-term impact on radiative forcing by generating ozone and perturbing sulphate oxidation; they also have a longer-term impact by changing the methane lifetime. The short-term impacts on ozone $F^{O_3}_i$ and sulphate $F^{SO_4}_i$ forcing are diagnosed from the equilibrium experiments perturbing emissions of species i but holding methane fixed. For $H \gg \alpha$, as for the aerosols, the AGWPs for the short-lived components are then simply $(F^{O_3}_i + F^{SO_4}_i)/E_i$. The longer-term impacts are diagnosed from the change in methane lifetimes with the perturbed emissions $\Delta\alpha^{CH_4}_i$. For small perturbations these can be shown to be equivalent to methane emissions of $\frac{\Delta\alpha^{CH_4}}{\alpha^{CH_4}} \frac{B^{CH_4}_0}{\alpha^{CH_4}}$ where $B^{CH_4}_0$ is the unperturbed burden (4983 Tg in the HTAP study). Hence the AGWP for ozone precursors including the short and long-term components is given by

$$\text{AGWP}^i = \frac{1}{E_i}\left(F^{O_3}_i + F^{SO_4}_i\right) + \chi_i \text{AGWP}^{CH_4}(H), \quad (2)$$

where the scaling factor $\chi_i = \frac{1}{E_i} \frac{\Delta\alpha^{CH_4}_i}{\alpha^{CH_4}} \frac{B^{CH_4}_0}{\alpha^{CH_4}}$. Note only the long-term components are functions of the time horizon. The GWPs at 20 and 100 yr for the ozone precursors were presented in Fry et al. (2012), Table S2.

ACPD
12, 23261–23290, 2012

3.2 Global temperature-change potentials

The absolute global temperature-change potential (AGTP) is given by the temperature response following an instantaneous pulse emission. The global surface temperature responds to changes in the radiative forcing at the tropopause on a spectrum of timescales. We follow the same methodology in Fuglestvedt et al. (2010) and use a temperature response function that is the sum of two exponentials $R(t) = \sum_{j=1}^{2} \frac{c_j}{d_j} \exp\left(-\frac{t}{d_j}\right)$ where the coefficients c_j and d_j are the climate sensitivities and timescales of the two modes. From Boucher and Reddy (2008) we use $c_1 = 0.631\,\mathrm{K(W\,m^{-2})^{-1}}$, $c_2 = 0.429\,\mathrm{K(W\,m^{-2})^{-1}}$, $d_1 = 8.4\,\mathrm{yr}$, $d_2 = 409.5\,\mathrm{yr}$, giving an equilibrium climate sensitivity of $1.060\,\mathrm{K(W\,m^{-2})^{-1}}$ (3.9 K for CO_2 doubling). The more common metrics are the GTPs which are normalised by the corresponding AGTP for CO_2. For this we use the expression in Fuglestvedt et al. (2010) (their Eq. A3).

$$\mathrm{AGTP}^{\mathrm{CO_2}}(H) = A^{\mathrm{CO_2}} \sum_{j=1}^{2} \left\{ a_0 c_j \left(1 - \exp\left(-\frac{H}{d_j}\right)\right) + \sum_{i=1}^{3} \frac{a_i \alpha_i^{\mathrm{CO_2}} c_j}{\alpha_i - d_j} \left(\exp\left(-\frac{H}{\alpha_i^{\mathrm{CO_2}}}\right) - \exp\left(-\frac{H}{d_j}\right)\right)\right\} \quad (3)$$

Here $A^{\mathrm{CO_2}}$ is the radiative efficiency for CO_2 in $\mathrm{W\,m^{-2}\,kg^{-1}}$, a_{0-3} are unitless coefficients [0.217,0.259, 0.338 and 0.186], and $\alpha_{1-3}^{\mathrm{CO_2}}$ are CO_2 response timescales [172.9, 18.51, 1.186] yr.

For aerosols with lifetimes much less than the time horizons of interest and the shortest climate timescale ($\alpha \ll H$, $\alpha \ll d_1$) the AGTP is simply a scaling of the climate response function by the equilibrium forcing from a unit step change in emission

$$\mathrm{AGTP}^{i}(H) = \frac{F_i}{E_i} R(H) = \mathrm{AGWP}^{i} \times R(H)$$

ACPD
12, 23261–23290, 2012

The GTP is calculated by dividing this by $AGTP^{CO_2}$. The GTPs for the 3 HTAP aerosol species from 4 continents separately and combined ("All") are shown in Fig. 1 for a 20 yr time horizon. The values for a 100 yr time horizon would have exactly the same pattern, but scaled by $R(100)/R(20) \times AGTP^{CO_2}(20)/AGTP^{CO_2}(100)(= 0.138)$. The patterns are also the same as for the AGWPs in Table 1 and the NDRFs in Yu et al. (2012).

For methane the interactions between the methane lifetime and the climate response timescales become important. Combining the expression for the methane AGWP with Eq. (A4) from Fuglestvedt et al. (2010) we get for the total AGTP:

$$AGTP^{CH_4}(H) = \left(F^{CH_4}_{CH_4} + F^{O_3}_{CH_4} + F^{SO_4}_{CH_4} + F^{H_2O}_{CH_4}\right) \frac{f\alpha^{CH_4}}{\Delta B^{CH_4}} \cdot \sum_{j=1}^{2} \frac{c_j}{f\alpha^{CH_4} - d_j} \left(\exp\left(\frac{-H}{f\alpha^{CH_4}}\right) - \exp\left(\frac{-H}{d_j}\right)\right) \quad (4)$$

The AGTPs for the other ozone precursor species can be calculated by combining the equilibrium responses with the effects on the methane lifetime to obtain an analogous expression to the AGWP:

$$AGTP^{i}(H) = \frac{1}{E_i}\left(F^{O_3}_{i} + F^{SO_4}_{i}\right) R(H) + \chi_i AGTP^{CH_4}(H) \quad (5)$$

The time evolution of the total AGTPs therefore depends on the relative balance between the short and long-term components. Figure 2 shows the GTP for NO_x, NMVOC and CO emissions (summed over the 4 continents). For NO_x emissions the long-term component acts in the opposite sense to the short-term (χ_i is negative). The AGTP starts positive, but becomes negative after 10 yr. For NMVOC and CO emissions the short-term and long-term components have the same sign, with the long-term component being relatively more important for CO. In all cases the GTP is dominated by the long-term component from about 30 yr to 60 yr. Beyond 60 yr the short and long-term components are of similar magnitudes, although both are very small. The results of

ACPD
12, 23261–23290, 2012

this can be seen in the bar charts of Fig. 3 which breaks the GTPs down by emission species and emission region. The net NO_x GTPs are negative with the largest impact coming from emissions in the South Asian region, and least impact from the European region. For VOCs the largest impact is also from the South Asian region whereas for CO the climate impact is largely independent of emission region. The fractional contribution to the GTP made by the methane response is greater for the 20 yr time horizon than the 100 yr horizon. The short-term contributions to the GTPs decline by a factor of 7.2 from 20 yr to 100 yr, but the long-term contributions decline by a factor of 15. The error bars are a combination of the uncertainties in $F_i^{O_3}$, $F_i^{SO_4}$, α^{CH_4}, and $\Delta\alpha_i^{CH_4}$ from the inter-model variability. For the non-methane precursors the dominant contribution comes from the inter-model variability in the changes to the methane lifetime ($\Delta\alpha_i^{CH_4}$). For methane the dominant contribution comes from the inter-model variability in the methane lifetime in the control run (α^{CH_4}). The direct methane contribution to the GTP(20) and GTP(100) are in agreement with Boucher et al. (2009), however the ozone contribution is slightly lower here, contributing 21 % to the methane GTP rather than the 25 % assumed in Boucher et al. (2009).

4 Regional climate change

Shindell and Faluvegi (2009), Shindell and Faluvegi (2010) and Shindell (2012) introduced the idea of the absolute regional temperature-change potential (ARTP) to quantify regional climate change from heterogeneous forcing patterns. There is not a one-to-one correspondence between the forcing in a region and the local temperature response as there are also contributions from the radiative forcing from outside the region due to the transport of heat. Shindell and Faluvegi (2009) showed that the forcing-temperature relationship could be characterised using 4 broad latitude bands: southern mid-high latitudes (90° S–28° S), tropics (28° S–28° N), northern mid-latitudes (28° N–60° N), and the Arctic (60° N–90° N). Thus the expression for the AGTP can be

ACPD
12, 23261–23290, 2012

generalised for heterogeneous forcing as:

$$\mathrm{ARTP}_m(H) = \sum_l \int_0^H k_{lm} \frac{F_l(t)}{E} R(H-t)\mathrm{d}t$$

where ARTP_m is the temperature response in latitude band m, k_{lm} are the response coefficients derived in Shindell and Faluvegi (2010) normalised by the climate sensitivity and F_l is the tropopause radiative forcing in latitude band l for a pulse emission E. We assume that the climate response function R applies equally to each region. As discussed in Shindell and Faluvegi (2010) in the different latitude bands encompassing such diverse regions as the Arctic and the tropics, the partitioning between the fast and slow response and even the time constants of these responses may vary from the global average, but there is no data currently available to break this down further.

For aerosol or methane emissions, the ARTPs have the same functional form as the AGTPs with the magnitudes given by the product of the response coefficients with the forcing pattern. The temperature change in latitude band m due to the emission of species i:

$$\mathrm{ARTP}^i_m(H) = \sum_l \frac{F_{i,l}}{F_i} k_{lm} \mathrm{AGTP}^i(H)$$

where F_i is the equilibrium globally-average forcing as before, and $F_{i,l}$ is the radiative forcing averaged over latitude band l. For methane $F_{\mathrm{CH_4},l} = F^{\mathrm{CH_4}}_{\mathrm{CH_4},l} + F^{\mathrm{O_3}}_{\mathrm{CH_4},l} + F^{\mathrm{SO_4}}_{\mathrm{CH_4},l}$, noting that the direct methane forcing and indirect forcings through ozone and sulphate will have different latitudinal distributions. We do not include the stratospheric water vapour forcing here as we have no information on its latitudinal profile. The latitudinal patterns of the ARTPs for aerosols or methane do not vary with time. Figure 4 shows the normalised equilibrium forcing patterns ($F_{i,l}/E_i$) and the $\mathrm{ARTP}^i_m(20)$ values for the 3 HTAP aerosol species. Note that for the scattering aerosols (SO_2 and POM emissions) the

ACPD
12, 23261–23290, 2012

largest radiative forcing is in the latitude band closest to the emitting region (28°–60° N for EA, EU and NA emissions, 28° S–28° N for SA emissions). There seems to be very little radiative forcing from scattering aerosols over the bright Arctic latitudes as there is less contrast between the brightness of the aerosol and the underlying albedo. For the absorbing aerosol (BC), due to the high contrast, the forcing is high over the Arctic latitudes and for EU emissions the Arctic response exceeds that of the northern mid-latitudes. The effect of applying the matrix of response coefficients is to smooth out the impacts such that there is less latitudinal variation in the temperature responses than in the forcing responses. However the Arctic temperatures are particularly sensitive to forcing changes in the northern mid-latitudes (at least in the coefficient set used here), so that the Arctic responses to the scattering aerosols are comparable to the northern mid-latitude responses. For the absorbing aerosol the Arctic shows the largest temperature response to BC emissions in any of the 4 continents. The ARTP(20) values are shown, but the latitudinal patterns will be identical for any time horizon, albeit with different overall scaling. The aerosol impacts on the northern latitudes are up to twice that implied just using the global average. The "global" ARTP bars are slightly larger than the calculated AGTPs in the previous section. This can be considered as an efficacy larger than unity due to the forcing being concentrated at the higher northern latitudes where the climate response is stronger.

For non-methane ozone precursors the ARTPs are a combination of two functional forms:

$$\mathrm{ARTP}^{i}_{m}(H) = \frac{1}{E_i} \sum_{l} \left(k_{lm} \left(F^{\mathrm{O_3}}_{i,l} + F^{\mathrm{SO_4}}_{i,l} \right) \right) R(H) + \chi_i \mathrm{ARTP}^{\mathrm{CH_4}}_{m}(H).$$

Here because the latitudinal patterns of the $F_{i,l}$ and $F_{\mathrm{CH_4},l}$ are different the overall spatial pattern of the ARTP evolves over time.

Figure 5 shows the latitudinal components of the forcing patterns for each ozone precursor from each region. The top panel shows the normalised short-lived equilibrium forcing terms $(F^{\mathrm{O_3}}_{i,l} + F^{\mathrm{SO_4}}_{i,l})/E_i$. The lower panel shows the total equilibrium forcing

ACPD
12, 23261–23290, 2012

patterns including the long-term component $(F_{i,l}^{O_3} + F_{i,l}^{SO_4})/E_i + \chi_i F_{CH_4,j}$ along with the forcing pattern for methane itself. The short-lived components give the highest response in the northern mid-latitudes for emissions from EA, EU and NA, and in the tropics for emissions from SA. For methane, the responses are more evenly distributed as methane is well-mixed, with the maximum forcing in the tropics, but a significant response in both the southern and northern extra-tropics. For NO_x, the χ_i are negative so the net forcing is the difference between short and long-term components. The net forcings are negative in the Southern Hemisphere and tropics where methane destruction outweighs the ozone production, but positive in the northern mid and high latitudes, except for SA emissions which only have a positive forcing in the northern mid-latitudes. For NMVOC and CO emissions, the χ_i are positive so the long and short-term components add. The latitudinal distributions for the total forcing become more even than for the short-term components. For CO, the highest response is in the tropics for all emission regions.

The corresponding ARTPs are shown in Fig. 6. For the ARTP(20)s, the long-term component is more important than the short-term component and the ARTPs for the non-methane ozone precursors look similar to the methane ARTP, with an opposite sign for NO_x emissions. The highest response is in the Arctic, again reflecting the sensitivity coefficients. For the ARTP(100) the contributions of the short and long-term components are more balanced. For NO_x the ARTP(100)s are positive in the northern mid to high latitudes for emissions from EA and NA reflecting the warming from ozone.

5 Limitations and uncertainties

The major limitations of this study are the neglect of aerosol-cloud interactions, nitrate aerosols and carbon cycle effects. The responses to aerosol emission changes were calculated using chemical transport models that omit interactions with clouds so the radiative forcings presented here only include direct effects based on the aerosol column

ACPD
12, 23261–23290, 2012

loadings (Yu et al., 2012). The indirect effects of aerosols are at least as great as the direct effect for hydrophilic aerosols (sulphate and POM in this study) and may also be important for black carbon. The indirect effects are likely to vary with emission region depending on their proximity to stratiform clouds.

NO_x emissions have an additional cooling effect by generating ammonium nitrate aerosols in regions of high ammonia abundance. Unfortunately nitrate aerosols were not included in many of the HTAP simulations, but we can use the results Bauer et al. (2007) who calculated a normalised direct radiative forcing from global anthropogenic NO_x emissions of -2.0×10^{-12} W m^{-2} kg^{-1}. This would add −25 to the NO_x GTP(20)s and −3.3 to the NO_x GTP(100)s, making these consistently negative.

However changes to the atmospheric composition of gases and aerosols can also affect the carbon cycle thus adding further indirect climate impacts (e.g. Sitch et al., 2007). Collins et al. (2010) showed that adding in the effects of surface ozone on vegetation damage added about 10 % to the methane GTP(20) and could change the sign of the NO_x GTPs. Hence the sign of the net impact of NO_x emissions is still uncertain.

Methane is oxidised in the atmosphere, with a molar fraction ε of between 0.5 and 1.0 resulting in CO_2 (Boucher et al., 2009). This provides an emission of CO_2 equal to $\varepsilon \times (44/16) \times [CH_4]/\alpha^{CH_4}$ which has its own climate impact (the factor 44/16 converts from a molar fraction to a mass fraction). Thus the addition to the methane GTP is:

$$\Delta AGTP^{CH_4}_{\text{oxidation}} = \int_0^H \varepsilon \times \frac{44}{16} \times \frac{1}{\alpha^{CH_4}} \exp\left(-\frac{t}{f\alpha^{CH_4}}\right) AGTP^{CO_2}(H-t)\mathrm{d}t$$

Note that for non-fossil methane this extra CO_2 is still produced as described above, but should be compensated for by previous uptake of CO_2. To do this would require detailed life-cycle analysis (for instance of the production of cattle fodder).

The temperature changes calculated in the GTPs can also lead to an impact on the carbon cycle, for instance through increased soil respiration. The definition of GTP for species i as a ratio $AGTP^i/AGTP^{CO_2}$ treats this inconsistently (the GWPs suffer

ACPD
12, 23261–23290, 2012

similarly). The temperature-carbon cycle feedback is implicitly included in the response function for CO_2 (Joos and Bruno, 1996) and hence in the denominator $AGTP^{CO_2}$, but is excluded in the numerator $AGTP^{i}$. Gillett and Matthews (2010) and Sarofim (2012) using carbon cycle models find that this can underestimate the GTPs for methane by 20%. A way of obtaining a simple estimate of this effect is to make the crude assumption that the change in the land-atmosphere flux of CO_2 is linearly proportionally to the surface temperature change with a coefficient γ. Multi-model comparisons of carbon cycle models (Friedlingstein et al., 2006; Arora et al., 2012) suggest a change in the land and ocean uptake of approximately $-1\,\mathrm{GtC\,yr^{-1}}$ per K temperature change. We therefore use a γ of $+(44/12)\times10^{12}\,\mathrm{kg(CO_2)\,yr^{-1}\,K^{-1}}$ with an uncertainty of 100 %. Treating this as an extra emission of $\gamma \times AGTP^{i}$ gives an addition to the AGTP due to the climate-carbon cycle feedback of:

$$\Delta AGTP^{i}_{\text{climate}} = \int_0^H \gamma AGTP^{i}(t) AGTP^{CO_2}(H-t)\mathrm{d}t$$

Note that because the $AGTP^{CO_2}$ does include the climate feedback we don't need to iterate this calculation any further. The contributions to the methane GTP from methane oxidation and climate-carbon cycle feedback are illustrated in Fig. 7 along with the direct methane impact (i.e. excluding ozone, sulphate and stratospheric water vapour). The methane oxidation adds 1.3 ± 0.4 and 2.1 ± 0.7 to the GTP(20) and GTP(100) respectively as in Boucher et al. (2009). The climate feedback effects are potentially larger at 1.7 ± 1.7 and 6.5 ± 6.5. The CO_2 impacts are more important at the longer timescales as they persist for considerably longer than the methane direct effect. This is particularly true for the climate feedback since the CO_2 continues to be emitted for some time after the original methane pulse has decayed.

One major uncertainty is in the assumptions about the climate response, both the timescales of the climate response function R and the latitudinal patterns included in the k_{lm}. Olivié and Peters (2012) explore the sensitivity of GTP to uncertainty in R

ACPD
12, 23261–23290, 2012

and find that uncertainties increase with time horizon and decrease with lifetime. For GTP^{CH_4} an uncertainty of −9/+8 % was found for a 20 yr time horizon, which increased to ±52 % for a time horizon of 100 yr (for 10th–90th percentiles). Higher uncertainty ranges were calculated for short-lived species such as aerosols; for 20 yr time horizon these were −39/ + 64 % and −64/ + 52 % for 100 yr (10th–90th percentiles).

6 Conclusions

We have examined the climate impacts of aerosols and reactive gas emissions from 4 continents as provided by chemistry transport models participating in the HTAP assessment. The radiative forcings and GWPs for the reactive gas emissions were previously documented in Fry et al. (2012), and the radiative forcings for the aerosols were documented in Yu et al. (2012). In this study we have moved further down the chain of climate impacts, showing how analytical formulae can be used to relate equilibrium radiative forcing values to the evolution of temperature changes using the GTP metric. We have also broken down the temperature changes by latitude band.

For the aerosol species the impacts of the emission changes are very rapid (< 1 yr) so the chain from RF to GWP to GTP adds little extra information since they are simply scalings of each other. Hence the relative importance of the emissions of the different species from different regions remains unchanged from Yu et al. (2012). The inter-model variability is larger than the variability between emission regions, suggesting that a single average metric would be a usable approximation. The small differences that are suggested are a lower climate impact for the scattering aerosols from East Asia, and a higher climate impact for the black carbon aerosols from Europe.

The reactive gas emissions perturb the atmospheric composition on two timescales, the first is again smaller than a year, the second is due to effects on the methane lifetime and has a characteristic timescale of 11.7 ± 1.8 yr. The relative importance of the short and long-term components varies with the time horizon used. This is most

ACPD
12, 23261–23290, 2012

noticeable for NO_x emissions where the short and long-term components act in opposite directions.

The different patterns of responses when moving down the impact chain becomes more apparent when breaking down the temperature changes into latitude bands. There is not a direct relationship between the radiative forcing in a region and the surface temperature change in that region. Even when using broad latitude bands there are contributions to the surface temperature from radiative forcing outside the region, although that contribution decreases with latitudinal distance. Thus the latitudinal temperature patterns can differ significantly from the global mean, and also from the latitudinal forcing patterns. For the aerosols the northern mid-latitude temperature response to northern mid-latitude emissions is approximately twice as large as the global average. This moves towards addressing an important policy question of whether emissions controls within a region have a larger climate effect in that region. For NO_x emissions, the responses in the northern mid-high latitude temperature changes are of different signs after 20 and 100 yr.

Acknowledgements. W. Collins was supported by the Joint DECC/Defra Met Office Hadley Centre Climate Programme (GA01101) and the Defra contract AQ0902. H. Yu was supported by NASA grant NNX11AH66G, managed by R. Eckman. J. S. Fuglestvedt's contribution was funded by the Norwegian Research Council within the project "Climate and health impacts of Short-Lived Atmospheric Components (SLAC)".

References

Arora, V. K., Boer, G. J., Friedlingstein, P., Eby, M., Christian, J. R., Jones, C. D., Bonan, G., Bopp, L., Brovkin, V., Cadule, P., Hajima, T., Ilyina, T., Tjiputra, J. F., and Wu, T.: Carbon-concentration and carbon-climate feedbacks in CMIP5 Earth System models, J. Climate, submitted, 2012.

Bauer, S. E., Koch, D., Unger, N., Metzger, S. M., Shindell, D. T., and Streets, D. G.: Nitrate aerosols today and in 2030: a global simulation including aerosols and tropospheric ozone, Atmos. Chem. Phys., 7, 5043–5059, doi:10.5194/acp-7-5043-2007, 2007.

ACPD

12, 23261–23290, 2012

Berntsen, T. K., Fuglestvedt, J. S., Joshi, M. M., Shine, K. P., Stuber, N., Ponater, M., Sausen, R., Hauglustaine, D. A., and Li, L.: Climate response to regional emissions of ozone precursors: sensitivities and warming potentials, Tellus, 57B, 283–304, 2005

Berntsen, T., Fuglestvedt, J., Myhre, G., Stordal, F., and Berglen, T. F.: Abatement of greenhouse gases: does location matter?, Clim. Change, 74, 377–411, 2006.

Bond, T. C., Zarzycki, C., Flanner, M. G., and Koch, D. M.: Quantifying immediate radiative forcing by black carbon and organic matter with the Specific Forcing Pulse, Atmos. Chem. Phys., 11, 1505–1525, doi:10.5194/acp-11-1505-2011, 2011.

Boucher, O. and Reddy, M. S.: Climate trade-off between black carbon and carbon dioxide emissions, Energ. Pol., 36, 193–200, 2008.

Boucher, O., Friedlingstein, P., Collins, W. J., and Shine, K. P.: Indirect GWP and GTP due to methane oxidation, Environ. Res. Lett., 4, 044007, doi:10.1088/1748-9326/4/4/044007, 2009.

Collins, W. J., Sitch, S., and Boucher, O.: How vegetation impacts affect climate metrics for ozone precursors, J. Geophys. Res., 115, D23308, doi:10.1029/2010JD014187, 2010.

Felzer, B. S., Cronin, T., Reilly, J. M., Melilloa, J. M., and Wang, X. D.: Impacts of ozone on trees and crops, C. R. Geosci., 339, 784–798, doi:10.1016/j.crte.2007.08.008, 2007.

Fiore, A. M., Dentener, F. J., Wild, O., Cuvelier, C., Schultz, M. G., Hess, P., Textor, C., Schulz, M., Doherty, R. M., Horowitz, L. W., IMacKenzie, I. A., Sanderson, M. G., Shindell, D. T., Stevenson, D. S., Szopa, S., Van Dingenen, R., Zeng, G., Atherton, C., Bergmann, D., Bey, I., Carmichael, G., Collins, W. J., Duncan, B. N., Faluvegi, G., Folberth, G., Gauss, M., Gong, S., Hauglustaine, D., Holloway, T., Isaksen, I. S. A., Jacob, D. J., Jonson, J. E., Kaminski, J. W., Keating, T. J., Lupu, A., Marmer, E., Montanaro, V., Park, R. J., Pitari, G., Pringle, K. J., Pyle, J. A., Schroeder, S., Vivanco, M. G., Wind, P., Wojcik, G., Wu, S., and Zuber A.: Multimodel estimates of intercontinental source-receptor relationships for ozone pollution, J. Geophys. Res., 114, D04301, doi:10.1029/2008JD010816, 2009.

Forster, P., Ramaswamy, V., Artaxo, P., Berntsen, T., Betts, R., Fahey, D., Haywood, J., Lean, J., Lowe, D., Myhre, G., Nganga, J., Prinn, R., Raga, G., Schulz, M., and Dorland, R. V.: Changes in atmospheric constituents and in radiative forcing, in: Climate Change 2007: The Physical Science Basis. Contribution of Working Group I to the Fourth Assessment Report of the Intergovernmental Panel on Climate Change, edited by: Solomon, S., Qin, D., Manning, M., Chen, Z., Marquis, M., Averyt, K. B., Tignor, M., and Miller, H. L., Cambridge University Press, Cambridge, UK and New York, NY, USA, 2007.

ACPD

12, 23261–23290, 2012

Friedlingstein, P., Cox, P., Betts, R., Bopp, L., von Bloh, W., Brovkin, V., Cadule, P., Doney, S., Eby, M., Fung, I., Bala, G., John, J., Jones, C., Joos, F., Kato, T., Kawamiya, M., Knorr, W., Lindsay, K., Matthews, H.D., Raddatz, T., Payner, P., Reick, C., Roeckner, E., Schnitzler, K. G., Schnur, R., Strassmann, K., Weaver, A. J., Yoshikawa, C., and Zeng, N.: Climate-carbon cycle feedback analysis, results from the C4MIP model intercomparison, J. Climate, 19, 3337–3353 doi:10.1175/JCLI3800.1, 2006.

Fry, M. M., Naik, V., West, J. J., Schwarzkopf, M. D., Fiore, A. M., Collins, W. J., Dentener, F. J., Shindell, D. T., Atherton, C., Bergmann, D., Duncan, B. N., Hess, P., MacKenzie, I. A., Marmer, E., Schultz, M. G., Szopa, S., Wild, O., and Zeng, G..: The influence of ozone precursor emissions from four world regions on tropospheric composition and radiative climate forcing, J. Geophys. Res., 117, D07306, doi:10.1029/2011JD017134, 2012.

Fuglestvedt, J. S., Berntsen, T. K., Isaksen, I. S. A., Mao, H. T., Liang, X. Z., and Wang, W. C.: Climatic forcing of nitrogen oxides through changes in tropospheric ozone and methane; global 3-D model studies, Atmos. Environ., 33, 961–977, doi:10.1016/S1352-2310(98)00217-9, 1999.

Fuglestvedt, J. S., Shine, K. P., Berntsen, T., Cook, J., Lee, D. S., Stenke, A., Skeie, R. B., Velders, G. J. M., and Waitz, I. A.: Transport impacts on atmosphere and climate: metrics, Atmos. Environ., 44, 4648–4677, doi:10.1016/j.atmosenv.2009.04.044, 2010.

GFDL Global Atmospheric Model Development Team (GAMDT): The new GFDL global atmosphere and land model AM2-LM2: evaluation with prescribed SST simulations, J. Clim., 17, 4641–4673, 2004.

Gillett, N. and Matthews, H.: Accounting for carbon cycle feedbacks in a comparison of the global warming effects of greenhouse gases, Environ. Res. Lett., 5, 034011, doi:10.1088/1748-9326/5/3/034011, 2010.

HTAP: Hemispheric Transport of Air Pollution 2010 – Part A: Ozone and Particulate Matter, Air Pollution Studies No. 17, edited by: Dentener, F., Keating, T., and Akimoto, H., United Nations, New York and Geneva, 2010.

Joos, F. and Bruno, M.: Pulse response functions are cost-efficient tools to model the link between carbon emissions, atmospheric CO_2 and global warming, Phys. Chem. Earth, 21, 471–476, 1996.

Naik, V., Mauzerall, D., Horowitz, L., Schwarzkopf, M. D., Ramaswamy, V., and Oppenheimer, M.: Net radiative forcing due to changes in regional emissions of tropospheric ozone precursors, J. Geophys. Res., 110, D24306, doi:10.1029/2005JD005908, 2005.

ACPD
12, 23261–23290, 2012

Olivié, D. J. L. and Peters, G. P.: Impact of spread in CO_2 and temperature IRFs on emission metrics, Earth Syst. Dynam. Discuss., 3, 935–977, 2012.

Prather, M. J.: Time scales in atmospheric chemistry: theory, GWPs for CH_4 and CO, and runaway growth, Geophys. Res. Lett., 23, 2597–2600, doi:10.1029/96GL02371, 1996.

Ramaswamy, V., Boucher, O., Haigh, J., Hauglustaine, D., Haywood, J., Myhre, G., Nakajima, T., Shi, G. Y., and Solomon, S.: Radiative forcing of climate change, in: Climate Change 2001: The Scientific Basis. Contribution of Working Group I to the Third Assessment Report of the Intergovernmental Panel on Climate Change (Cambridge: Cambridge University Press) chapter 6, 350–416, 2001.

Sarofim, M. C.: The gtp of methane: modeling analysis of temperature impacts of methane and carbon dioxide reductions, Environ. Model. Assess., 17, 231–239, doi:10.1007/s10666-011-9287-x, 2012.

Shindell, D. T.: Evaluation of the absolute regional temperature potential, Atmos. Chem. Phys. Discuss., 12, 13813–13825, doi:10.5194/acpd-12-13813-2012, 2012.

Shindell, D. and Faluvegi G.: Climate response to regional radiative forcing during the twentieth century, Nature Geosci., 2, 294–300, doi:10.1038/NGEO473, 2009.

Shindell, D. and Faluvegi, G.: The net climate impact of coal-fired power plant emissions, Atmos. Chem. Phys., 10, 3247–3260, doi:10.5194/acp-10-3247-2010, 2010.

Shindell, D. T., Schulz, M., Ming, Y., Takemura, T., Faluvegi, G., and Ramaswamy, V.: Spatial scales of climate response to inhomogeneous radiative forcing, J. Geophys. Res., 115, D19110, doi:10.1029/2010JD014108, 2010.

Shine, K. P., Fuglestvedt, J. S., Hailemariam, K., and Stuber, N.: Alternatives to the global warming potential for comparing climate impacts of emissions of greenhouse gases, Clim. Change 68, 281–302, 2005.

Shine, K. P., Berntsen, T. K., Fuglestvedt, J. S., Skeie, R. B., and Stuber, N.: Comparing the climate effect of emissions of short and long lived climate agents, Phil. Trans. Roy. Soc. A, 365, 1903–1914, 2007.

Sitch, S., Cox, P. M., Collins, W. J., and Huntingford, C.: Indirect radiative forcing of climate change through ozone effects on the land-carbon sink, Nature, 448, 791–794, doi:10.1038/nature06059, 2007.

United Nations Environment Programme and World Meteorological Organization: "Integrated Assessment of Black Carbon and Tropospheric Ozone", Nairobi, 2011.

ACPD

12, 23261–23290, 2012

Yu, H., Dickinson, R. E., Chin, M., Kaufman, Y. J., Zhou, M., Zhou, L., Tian, Y., Dubovik, O., and Holben, B. N.: The direct radiative effect of aerosols as determined from a combination of MODIS retrievals and GOCART simulations, J. Geophys. Res., 109, D03206, doi:10.1029/2003JD003914, 2004.

Yu, H., Chin, M., West, J., Atherton, C. S., Bellouin, N., Bergmann, D., Bey, I., Bian, H., Diehl, T., Folberth, G., Hess, P., Shindell, D. T., Takemura, T., and Tan, Q.: A HTAP multi-model assessment of the influence of regional anthropogenic emission reductions on aerosol direct radiative forcing and the role of intercontinental transport, J. Geophys. Res., submitted, 2012.

ACPD

12, 23261–23290, 2012

Table 1. Absolute global warming potentials (AGWPs) for emissions of SO_2, POM and BC from the 4 HTAP continents, based on Table 6 of Yu et al. (2012). Units are $W\,m^{-2}\,yr\,kg^{-1}$.The AGWPs for aerosols are approximately independent of time horizon.

	EA	EU	NA	SA	All
SO_2	$-2.6 \pm 1.0 \times 10^{-12}$	$-3.6 \pm 1.1 \times 10^{-12}$	$-3.5 \pm 1.0 \times 10^{-12}$	$-3.6 \pm 0.8 \times 10^{-12}$	$-3.2 \pm 1.0 \times 10^{-12}$
OC	$-3.7 \pm 1.8 \times 10^{-12}$	$-4.3 \pm 1.7 \times 10^{-12}$	$-4.3 \pm 1.7 \times 10^{-12}$	$-4.2 \pm 1.8 \times 10^{-12}$	$-4.0 \pm 1.7 \times 10^{-12}$
BC	$30 \pm 20 \times 10^{-12}$	$39 \pm 18 \times 10^{-12}$	$29 \pm 15 \times 10^{-12}$	$25 \pm 15 \times 10^{-12}$	$31 \pm 17 \times 10^{-12}$

ACPD
12, 23261–23290, 2012

Table 2. GTPs at 20 and 100 yr time horizons for the HTAP aerosols (or precursors), methane and non-methane ozone precursors. Data are given for emissions from the 4 HTAP continents separately and combined. For methane only a global number is given. Uncertainties are inter-model differences in the CTM responses to emission perturbations from Yu et al. (2012) and Fry et al. (2012). This includes uncertainties in the aerosol and ozone responses, and in the methane lifetime response.

	EA	EU	NA	SA	All
			GTP(20)		
SO_2	−31 ± 13	−43 ± 15	−43 ± 14	−42 ± 9	−38 ± 12
POM	−50 ± 17	−58 ± 18	−59 ± 15	−58 ± 17	−55 ± 16
BC	410 ± 350	530 ± 190	400 ± 150	350 ± 160	420 ± 190
CH_4					54.6 ± 8.8
NO_x	−55.6 ± 23.8	−48.0 ± 14.9	−61.9 ± 27.8	−124.6 ± 67.4	−62.1 ± 26.2
NMVOC	8.4 ± 4.6	9.5 ± 6.5	8.6 ± 6.4	15.7 ± 5.0	10.0 ± 5.7
CO	3.5 ± 1.3	3.2 ± 1.2	3.7 ± 1.3	3.4 ± 1.0	3.5 ± 1.2
			GTP(100)		
SO_2	−4.1 ± 1.6	−5.7 ± 2.0	−5.7 ± 1.8	−5.5 ± 1.1	−5.1 ± 1.6
POM	−6.7 ± 2.0	−7.7 ± 2.4	−7.8 ± 2.0	−7.7 ± 2.3	−7.3 ± 2.1
BC	55 ± 46	71 ± 25	53 ± 20	46 ± 21	56 ± 25
CH_4					3.6 ± 1.2
NO_x	−1.3 ± 2.1	−2.5 ± 1.3	−1.7 ± 2.1	−4.6 ± 5.1	−2.2 ± 2.1
NMVOC	0.7 ± 0.4	0.8 ± 0.5	0.7 ± 0.5	1.3 ± 0.5	0.9 ± 0.5
CO	0.26 ± 0.12	0.24 ± 0.11	0.27 ± 0.12	0.27 ± 0.10	0.26 ± 0.11

ACPD
12, 23261–23290, 2012

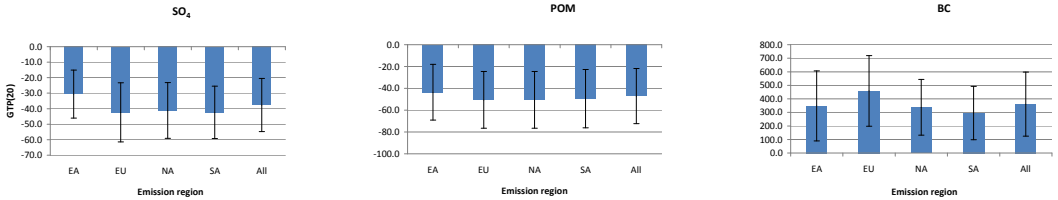

Fig. 1. GTP(20) for emissions of SO_2, POM and BC from the four HTAP continents. Error bars reflect 1 s.d. uncertainty in the multi-model responses.

ACPD
12, 23261–23290, 2012

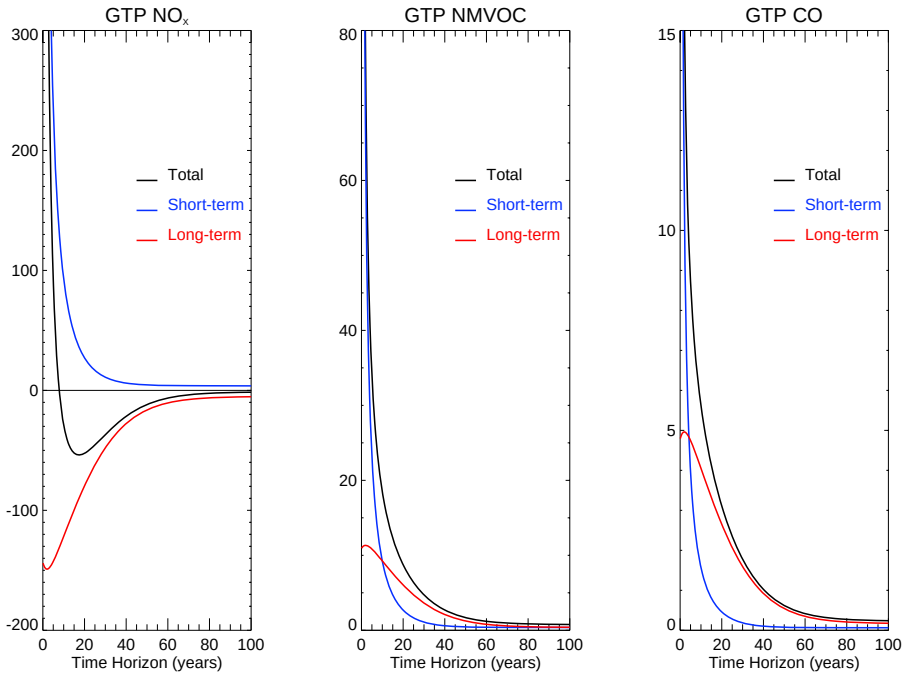

Fig. 2. GTPs as functions of time horizon for emissions of NO_x, NMVOC and CO from all 4 continents combined. The short and long-term components are also shown.

ACPD
12, 23261–23290, 2012

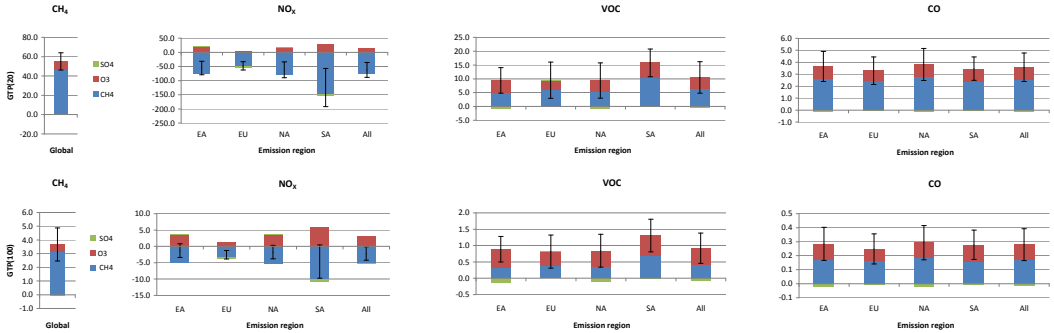

Fig. 3. GTP(20) and GTP(100) for emissions of CH_4, NO_x, VOC and CO from the four HTAP continents separately and combined ("All"). The GTPs are split according to the contributing components. For O_3 and SO_4 these combine both the short and long-term components. The contribution from stratospheric water vapour is included in with CH_4. Error bars reflect 1 standard deviation uncertainty in the multi-model responses.

ACPD
12, 23261–23290, 2012

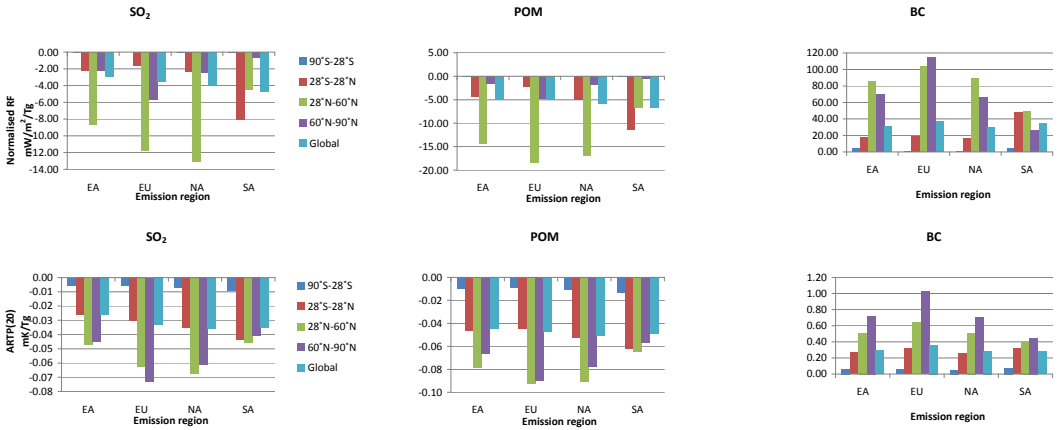

Fig. 4. Normalised equilibrium forcing in mW m^{-2} Tg^{-1} (upper panel) and ARTP(20) in mK Tg^{-1} (lower panel) for emissions of SO_2, POM and BC from the four HTAP continents. The coloured columns represent the responses in 4 different latitude bands (90° S–28° S, 28° S–28° N, 28° N–60° N, 60° N–90° N) and a global response.

ACPD
12, 23261–23290, 2012

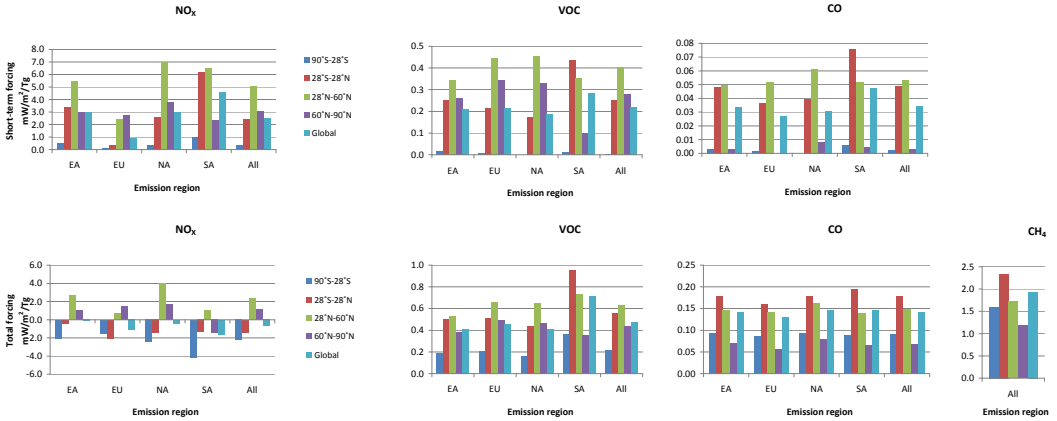

Fig. 5. Short-term (upper) and total (lower) normalised equilibrium forcing in $mW\,m^{-2}\,Tg^{-1}$ for emissions of CH_4, NO_x, VOC and CO from the four HTAP continents. The coloured columns represent the responses in 4 different latitude bands (90° S–28° S, 28° S–28° N, 28° N–60° N, 60° N–90° N) and a global response.

ACPD
12, 23261–23290, 2012

Global and regional temperature-change potentials for NTCFs

W. J. Collins et al.

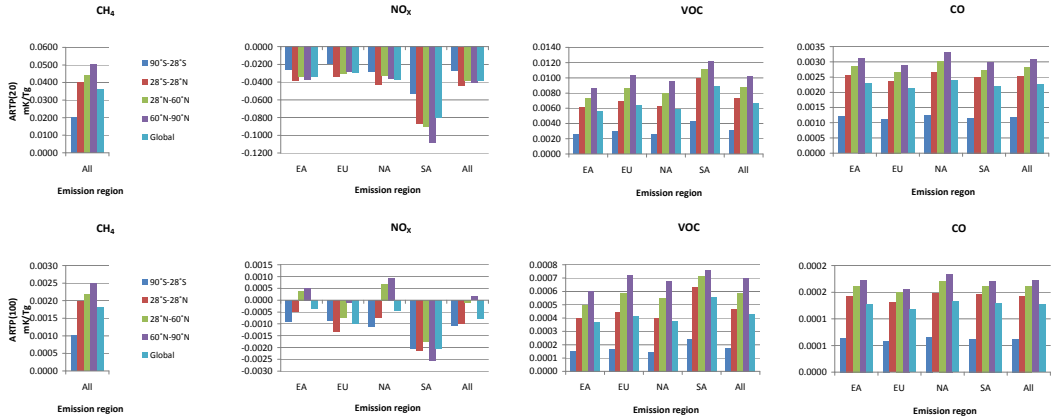

Fig. 6. ARTP(20) and ARTP(100) in mK Tg^{-1} for emissions of CH_4, NO_x, VOC and CO from the four HTAP continents. The coloured columns represent the responses in 4 different latitude bands (90° S–28° S, 28° S–28° N, 28° N–60° N, 60° N–90° N) and a global response.

ACPD
12, 23261–23290, 2012

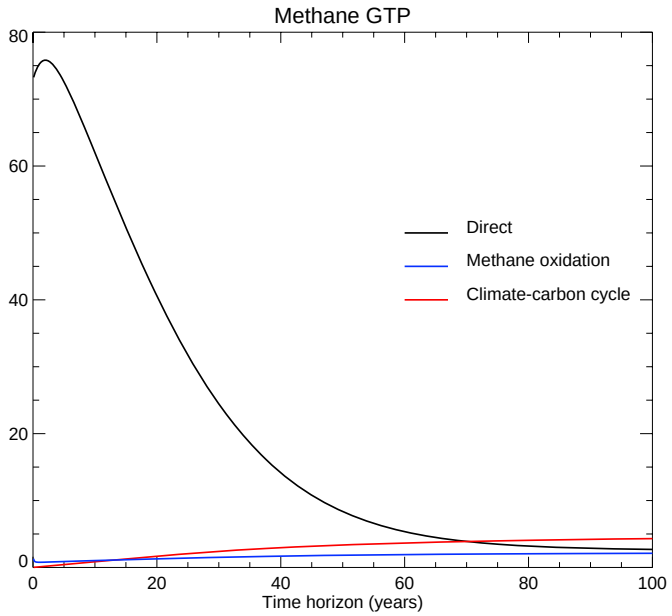

Fig. 7. The direct methane GTP (excluding ozone, sulphate and stratospheric water vapour), and additional contributions from CO_2 from two sources: the atmospheric oxidation of methane; and the impact of the methane-induced temperature change on the carbon cycle.

ACPD
12, 23261–23290, 2012